T. L. Naing, T. O. Rocheleau, and C. T.-C. Nguyen, "Simultaneous multi-frequency switchable oscillator and FSK modulator based on a capacitive-gap MEMS disk array," *Tech. Digest*, 2015 IEEE Int. Micro Electro Mechanical Systems Conference, Estoril, Portugal, Jan. 18-22, 2015, pp. 1024-1027.

SIMULTANEOUS MULTI-FREQUENCY SWITCHABLE OSCILLATOR AND FSK MODULATOR BASED ON A CAPACITIVE-GAP MEMS DISK ARRAY

Thura Lin Naing, Tristan O. Rocheleau, and Clark T.-C. Nguyen
University of California, Berkeley, USA

ABSTRACT

An electromechanical circuit constructed from array-composites of capacitive-gap micromechanical resonators with differing frequencies, wired in closed-loop feedback with a single ASIC amplifier, provides a first MEMS-based multi-frequency oscillator generating simultaneous oscillation outputs in the vicinity of 61 MHz. The use of only one amplifier for all frequencies (as opposed to one for each frequency) saves substantial power and is made possible by exploiting softening and damping non-linearities in the MEMS resonators, often considered a limitation, but here providing amplitude limiting that prevents amplifier desensitization to other frequencies. Furthermore, electrical stiffness-based frequency tuning enables Frequency-Shift Keyed (FSK) modulation of the output waveform, offering a space and power-efficient multichannel transmitter, as desired for mobile applications requiring long battery life, such as wireless sensor nodes. Indeed, while capable of multiple simultaneous and independent frequency outputs, this oscillator consumes only 137 μW, which is one-third that of previous multi-frequency efforts that only produce one frequency at a time [1].

INTRODUCTION

Wireless technology, which already plays a major part in our daily lives, is expected to expand to networks of billions of autonomous sensors in coming years: the so-called Internet of Things [2]. In one vision, sensors employing tiny, low-cost wireless motes collect and transmit data through a mesh network while operating only on scavenged or battery power. Here, small form-factor, spectrum efficient, low-power wireless communication links are essential. Vibrating RF MEMS technology, with already available products ranging from compact low-phase-noise MEMS-based reference oscillators [3, 4], to band-selecting RF front-end duplexers [5], offers a compelling potential route towards such a vision.

Indeed, capacitive-gap transduced MEMS resonators already offer space and power savings over conventional oscillators [3], where the high Q's >100,000 exhibited by these on-chip resonators allow for noise performance exceeding even the challenging GSM specifications with only ~100 μW of power consumption. MEMS-based radios [6] offer even more interesting possibilities, especially considering the low power and blocker resilience they provide in such small sizes. While impressive, these previous MEMS circuits have limited frequency tuning capability (~100 kHz range), and lack the ability to simultaneously communicate on separate channels.

Pursuant to solving these deficiencies, this work presents an oscillator (*cf.* Fig. 1) that combines a single amplifier with a plurality of MEMS resonators capable of not only outputting multiple independent frequencies in the vicinity of 61MHz; but also, by exercising voltage-controlled electrical stiffness tuning [7] of individual resonator array-composites, Frequency Shift Key (FSK) modulating each frequency to generate waveforms suitable for simultaneous wireless transmission in multiple channels. The chosen frequency is ideal for long-range unlicensed operation in the 52-74 MHz band white-space [8] and ISM bands at 27.12 MHz and 40.68 MHz [9].

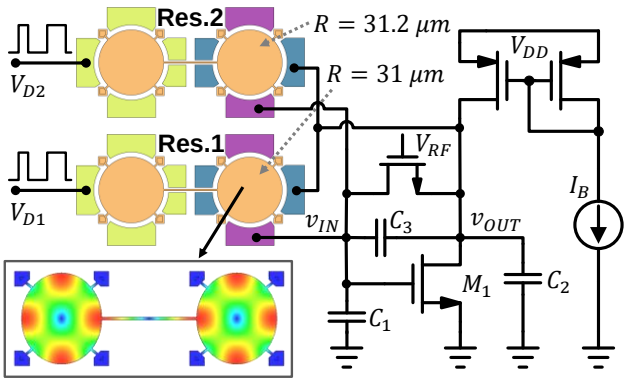

Fig. 1: Schematic of the Pierce topology multi-oscillator circuit used in this work. Independent tuning voltages and input bit streams are applied to Res. 1 and Res. 2. In each array-composite resonator, electrodes with the same color are electrically connected together. Inset shows FEM mode shape simulation of the two-disk array.

DEVICE DESIGN AND OPERATION

The multi-oscillator system here comprises two main parts: a sustaining amplifier circuit and a multi-frequency MEMS array-composite resonator circuit. The ability to use only one amplifier with multiple resonators saves considerable power and derives from the ability of MEMS resonators to limit the oscillation amplitude [10]. In particular, unlike the vast majority of oscillators in which the sustaining amplifier rails out to limit the oscillation amplitude, thereby desensitizing it to any other frequency; the multiple oscillation amplitudes (at different frequencies) of this MEMS oscillator limit via spring softening and damping nonlinearities in the MEMS resonators. This then allows the amplifier to remain linear and provide gain at multiple frequencies.

The use of array-composites, like that of Fig. 2, rather than just single resonators essentially allows for additional electrodes through which more control of the total array-composite resonator is obtained, e.g., for frequency pulling, strong input/output (I/O), "on/off" switching, etc. The Fig. 2 array-composite specifically uses wine-glass-mode disk resonators to take advantage of their ability to attain the needed frequencies while allowing accurate specification via CAD layout of multiple unique frequencies on the same die. Each resonator comprises a 2 μm-thick, ~31 μm-radius polysilicon disk supported by beams at quasi nodal points and electrically coupled along their sidewalls to input-output electrodes by tiny 50 nm capacitive gaps.

In each two-disk array-composite, a half-wavelength beam

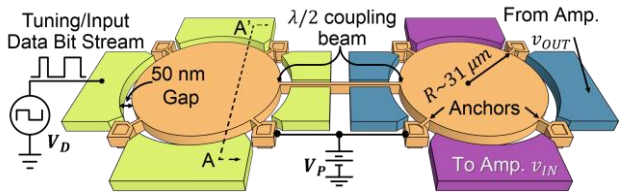

Fig. 2: Perspective view of a single MEMS two-disk array-composite comprising two suspended, mechanically-coupled disk resonators (orange) anchored at their 4 nodal points. Tuning electrodes (light green) on one disk allow for electronic frequency control while input (blue) and output electrodes (purple) on the second one connect to bus bars to provide a mulit-port multi-resonator device.

mechanically couples the disks, where sizing to half the acoustic wavelength forces the individual resonator disks to move in-phase at a single resonance frequency. Effectively, the array of disks behaves as one disk with twice the sidewall surface area with which to electrically interrogate or control it. To excite the composite resonator into motion, a bias voltage V_P on the disk structure combines with an ac drive voltage applied to the input electrodes (blue and labeled "From Amp") around the right-hand disk to produce forces across the input electrode-to-resonator gaps that, at resonance, excite the wine-glass (i.e., compound (2, 1)) mode shape, shown in the inset of Fig. 1. Here, disk radius R primarily sets the resonance frequency [11, 12]. A 0.2 μm difference in disk radii separates the Fig. 1 disk array-composite frequencies by 300 kHz around 61 MHz.

While the disk on the right provides the I/O interface (to the sustaining amplifier), the disk on the left enables control of frequency via the voltage-controllable electrical stiffness, which influences the frequency via [7, 12]:

$$f_{ot} = f_{nom}\sqrt{1-\frac{k_e}{k_{mre}}} \qquad (1)$$
$$f_{nom} = \frac{1}{2\pi}\sqrt{\frac{k_{mre}}{m_{mre}}};\ k_e = \frac{\alpha^2 C_o}{d_0^2}V_{PG}^2$$

where k_{mre} and m_{mre} are the effective dynamic mechanical stiffness and mass at the highest displacement location, k_e is the electrical stiffness, the C_o is the total electrode-to-resonator overlap capacitance of a disk, d_o is the gap spacing, V_{PG} is the bias voltage across the gap, and α is a dimensionless constant based on mode and electrode shape, equal to 0.787 for the design used here [12]. This effect enables both frequency tuning via adjustment of the voltage on tuning electrodes (green in Fig. 2) producing the typical tuning response shown in Fig. 3(a), as well as a simple FSK modulation of the steady-state oscillation to be discussed.

To shut an array-composite off, just set its V_P to zero.

OSCILLATOR DESIGN AND LIMITING

Upon connection of the I/O electrodes of two or more Fig. 2-like array-composites to a suitable sustaining amplifier, oscillation ensues for those devices given sufficiently large dc-bias voltages V_P's. Whether or not the V_P is large enough depends on the relative magnitude of the resulting motional resistance R_x of the array-composite in question versus the effective transresistance gain R_{amp} of the sustaining amplifier. If $R_{amp} > R_x$, oscillations start

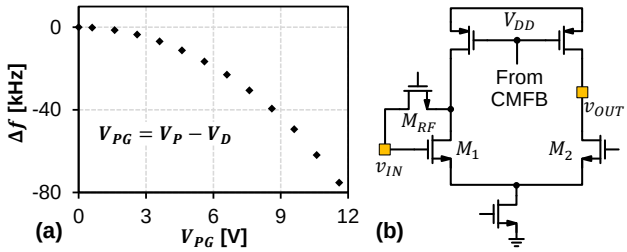

Fig. 3: (a) Oscillation frequency tuning vs. applied voltage across the capacitance gap of the tuning resonator. (b) TIA amplifier circuit schematic [6].

up and continue to grow until some form of nonlinearity reduces the loop gain to 1, at which point growth stops and steady-state oscillation ensues with a constant amplitude. In the vast majority of cases, including quartz crystal oscillators, electronic amplifier nonlinearity is responsible for limiting. However, unlike macroscopic resonators, the MEMS-based frequency setting element in the present oscillator can actually go nonlinear before the amplifier, at which point it ends up limiting the steady-state oscillation amplitude. Whether or not this happens depends upon the type and linearity of amplifier itself.

Amplifier Limiting

Among MEMS-based oscillator types, series resonant and Pierce topologies have been most popular and successful. Series resonant oscillators often employ TransImpedance Amplifiers (TIA's) [6], such as shown in Fig. 3(b), that amplify an input current to an output voltage by a gain factor set by the value of resistance simulated by the shunt-shunt feedback transistor M_{RF}. While the ability of this topology to cancel common-mode noise is beneficial [13], it exhibits stronger nonlinearity than alternative circuits, because: 1) it uses three stacked transistors between the supply and ground, which sacrifices output voltage swing; and 2) the resistance of the feedback transistor M_{RF} can vary significantly as the output voltage changes. As a result, a TIA-based series resonant oscillator generally limits oscillation at amplitudes smaller than required to incite sufficient resonator nonlinearity, i.e., the amplifier limits the oscillation, not the resonator.

Conversely, the simpler Pierce topology [3] of Fig. 1 allows larger output swings, as it has only two stacked transistors between the supply and ground and does not employ feedback. By staying linear under larger voltage swings, a Pierce topology makes possible the resonator-limited operation needed to achieve a multi-oscillator.

Resonator Limiting

The disk resonator nonlinearity responsible for limiting oscillator amplitude generally manifests as a combination of stiffness nonlinearity that generates the well-known Duffing response [14]; and damping nonlinearity that increases resonator loss at large displacement amplitudes. In MEMS-based resonators, Duffing nonlinearity appears as either a hardening nonlinearity typically caused by stress, where the frequency response bends forwards, i.e., towards higher frequencies; or a softening nonlinearity, caused in capacitive-gap transduced resonators by higher-order components of electrical stiffness that bend the frequency response backwards, i.e., towards lower frequencies.

For the tiny-gap disks of this work, the softening

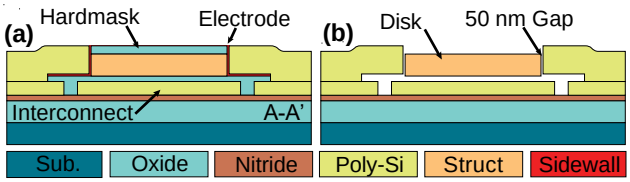

Fig. 4: Cross-sections of the fabricated disk resonators (a) before release and (b) after release in 49% HF.

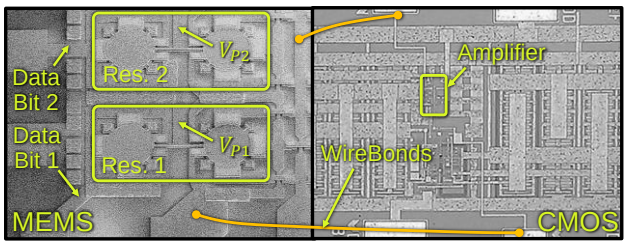

Fig. 5: SEMs of the fabricated MEMS circuit and die photo of the custom-made CMOS amplifier IC. Wirebond connections shown in orange.

nonlinearity dominates. Pursuant to modeling this nonlinearity, the differential equation governing resonator motion is

$$m_{mre}\frac{\partial^2 x}{\partial t^2} + (\gamma_0 + \eta x^2)\frac{\partial x}{\partial t} + kx + k_1 x^2 + \cdots$$
$$k_2 x^3 = \frac{\alpha C_o}{2d_0} V_{PG} v_{IN} \cos(\omega t) = F_\omega \cos(\omega t) \quad (2)$$

where F_ω is the magnitude of the drive force acting on the resonator, k_1 and k_2 model the softening nonlinearity derived from capacitive-gap interactions, η is an empirically-determined term describing non-linear damping [15], and

$$k = k_{mre} - 2k_e;\ k_1 = \frac{6k_e}{2d_0};\ k_2 = -\frac{4k_e}{d_0^2};\ \gamma_0 = \frac{\omega_o m_{mre}}{Q} \quad (3)$$

where Q is the resonator's unloaded quality factor, and $\omega_o = \sqrt{k/m_{mre}}$. Using the perturbation method of [15], this nonlinear system yields an approximate displacement amplitude as a function of frequency given by

$$X_0 = \frac{F_\omega/m_{mre}}{\sqrt{(\omega^2 - \omega_o'^2)^2 + (\omega\omega_o'/Q')^2}}$$
$$Q' = \frac{2\omega_o m_{mre}}{2\gamma_0 + \eta X_0^2};\ \omega_o' = \omega_o + \kappa . X_0^2;\ \kappa = \left[\frac{3k_2}{8k} - \frac{5k_1^2}{12k^2}\right]\omega_o \quad (4)$$

Equation (4) captures the drive amplitude-induced bending and peak lowering of the frequency response responsible for oscillator amplitude limiting.

EXPERIMENTAL RESULTS

Pursuant to demonstrating a multi-frequency oscillators and FSK-generator, two-disk array-composites like that of Fig. 2 were designed to operate around 61 MHz and fabricated using a process similar to that of [6] to achieve the final cross-section shown in Fig. 4. Here, $POCl_3$-doped polysilicon deposited via low-pressure chemical-vapor deposition (LPCVD) at 615 ºC provided all resonator structure, electrode, and electrical interconnect material. A high-temperature oxide (HTO) sidewall sacrificial deposition defined the 50-nm resonator-to-electrode gaps. Structures were released in 49% HF to yield the final test devices.

Amplifier ICs were designed and fabricated using a

Table 1: Design and Extracted Parameters of the Fabricated MEMS Resonator Array-Composite.

Q	40k	α	0.787	k_{mre}[N/m]	1.61×10^6
d_0[nm]	50	m_{mre}[pg]	11.33	k_e[N/m]	9.73×10^2
V_{PG}[V]	8.4	γ_0[N.s/m]	1.07×10^{-7}	k_1[N/m^2]	5.84×10^{10}
C_o[fF]	55.66	η[N.s/m^3]	4×10^8	k_2[N/m^3]	-1.56×10^{18}

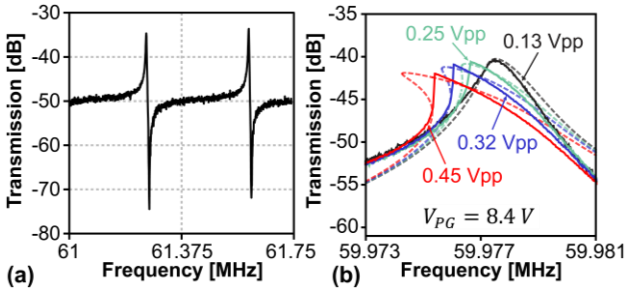

Fig. 6: (a) Frequency response as measured by an Agilent E5071C network analyzer for a two-disk array-composite with both resonators turned 'on' via applied bias voltage. (b) Measured (solid lines) and theoretical (dashed lines) spring softening and damping nonlinear response as a function of increasing drive voltage.

0.35 µm CMOS technology. To construct a complete multi-frequency oscillator, wire bonds connect released two-disk array-composites with the CMOS ASIC shown in Fig. 5, both of which are then mounted on a circuit board to provide needed bias and signal voltages.

Fig. 6(a) presents the frequency response of a two-disk array-composite under 10 V dc-bias and in vacuum. Fig. 6(b) presents the measured (solid lines) and theoretical (dotted lines, using (4)) the frequency response behavior of a single such disk with increasing drive voltage measured with forward going frequency, showing both spring softening (generating the saw-tooth shape) and damping (causing a decrease in peak height) nonlinearities. Again, the latter damping nonlinearity limits the oscillation amplitude. Here, the model can be seen to closely match measurement, verifying that capacitive-gap derived phenomena govern the stiffness non-linearity and that significant amplitude-limiting loss manifests when the drive voltage surpasses ~130 mVpp.

Fig. 7(a,b) present measured output spectra from a Pierce-based multi-oscillator like that of Fig. 1, where application or removal of V_P's ~10V on/off switch the MEMS array-composites sequentially. Fig. 7(c) and Fig. 8 demonstrate operation with bias applied to both resonators, showing two simultaneous oscillation frequencies, each independently amplitude-limited as expected when using the linear sustaining amplifier of a Pierce oscillators. Here, the ASIC operates off a 2.8 V supply drawing ~49 µA. To verify the need for MEMS-based amplitude limiting, Fig. 9 presents the output of another such oscillator built instead using the TIA of Fig. 3(b) designed to limit at drive amplitudes above 10 mVpp. Unlike the Pierce design, when both resonators are "on", one of them grows in amplitude faster than the other and causes amplifier-induced (rather than resonator-induced) limiting, desensitizing the amplifier to other frequencies, and making it impossible to achieve the desired multi-frequency output.

Finally, to gauge the efficacy of this mechanical circuit as a multi-channel transmitter, Fig. 10 presents the output

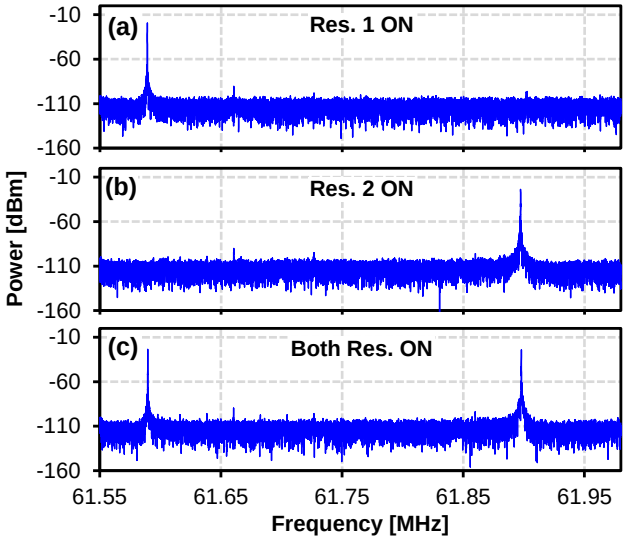

Fig. 7: Pierce oscillator output spectra measured on an Agilent N9030A spectrum analyzer. (a) shows oscillator output with resonator 1 turned on via an applied bias of 9.35 V, (b) with 11.6 V applied to resonator 2, and (c) simultaneous oscillation with bias voltages applied to both.

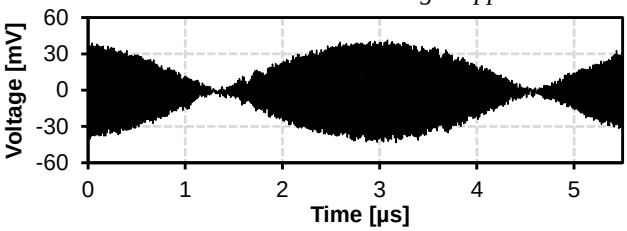

Fig. 8: Measured oscillator output waveform of the Pierce-based circuit with two resonators active.

with one oscillator active with a binary FSK input signal applied to the tuning electrode of its array-composite. This realizes electrical stiffness-induced switching of the oscillator frequency, thereby producing the fast-response, continuous-phase FSK modulation shown, at a minimum-shift keyed bitrate of 40 kbps.

CONCLUSIONS

The multi-frequency oscillator in this work is the first of its kind to generate simultaneous oscillation outputs around 61 MHz using capacitive-gap MEMS resonator array-composites while employing only a single amplifier. This MEMS-based circuit provides not only independently switchable and tunable oscillation outputs at multiple frequencies, but also a multi-channel FSK transmitter, all in a power- and space-saving package commensurate with the needs of long-term mobile applications, such as wireless sensor nodes. The ability to simultaneously transmit on multiple channels using only one amplifier enables a high degree of wireless multiplexing with substantially less power than competing multi-amplifier approaches—clearly desirable for tomorrow's autonomous wireless networks.

Acknowledgement: This work was supported by DARPA.

REFERENCES

[1] M. Rinaldi, *et al.*, "Reconfigurable …," *IEEE Tran. on Electron Devices*, vol. 58, no. 5, pp. 1281-1286, May 2011.
[2] "Facts and Forecasts: Billions of Things, Trillions of Dollars," [Online]. Available: http://www.siemens.com.
[3] T. L. Naing, *et al.*, "A 78-microwatt GSM phase noise-compliant…," in *Proceedings, IFCS*, 2013, pp. 562-565.
[4] H. Lee, *et al.*, "Low Jitter and Temperature Stable MEMS Oscillators," in *Proceedings, IFCS*, 2012, pp. 271-275.
[5] Avago, LTE Band 7 Duplexer, Part No. ACMD-6007.
[6] T. O. Rocheleau, *et al.*, "A MEMS-based tunable RF channel...," in *Tech. Digest, Hilton-Head Conf.*, 2014.
[7] H. C. Nathanson, *et al.*, "The resonant gate…," *IEEE Trans. on Electron Devices*, vol. 14, no. 3, pp. 117- 133, Mar. 1967.
[8] "FCC, Et Docket No. 08-260, Second Report and Order," 2008. Available: http://hraunfoss.fcc.gov/edocs_public/attachmatch/DOC-286566A1.pdf.
[9] "FCC Online Table of Frequency Allocations," [Online]. Available: http://transition.fcc.gov.
[10] S. Lee, *et al.*, "Phase noise amplitude dependence in self-limiting …," in in *Tech. Digest, Hilton-Head Conf.*, 2004.
[11] M. Onoe, "Contour vibrations of isotropic …," *J. Acoust. Soc. Amer.*, vol. 28, no. 6, p. 1158–1162, Nov. 1956.
[12] M. Akgul, *et al.*, "A negative capacitance …," *IEEE Trans. on UFFC*, vol. 61, no. 5, pp. 849-869, May 2014.
[13] Y.-W. Lin, *et al.*, "Series-resonant VHF micromechanical …," *IEEE JSSC*, vol. 39, no. 12, pp. 2477-2491, Dec. 2004.
[14] G. Duffing, Erzwungene Schwingungen bei veranderlicher Eigenfrequenz und ihre …: Vieweg & Sohn, 1918.
[15] R. Lifshitz, *et al.*, "Nonlinear …," in *Reviews of Nonlinear Dynamics and Complexity*, Wiley, 2009, pp. 1-52.

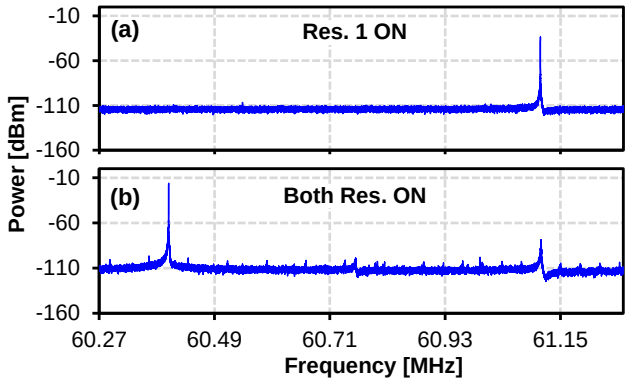

Fig. 9: TIA-based oscillator output spectra with (a) one resonator turned on and (b) both resonators on and loop gain increased by ~30% in an attempt to produce simultaneous oscillation. Oscillation at one frequency desensitizes the TIA, suppressing output at the other.

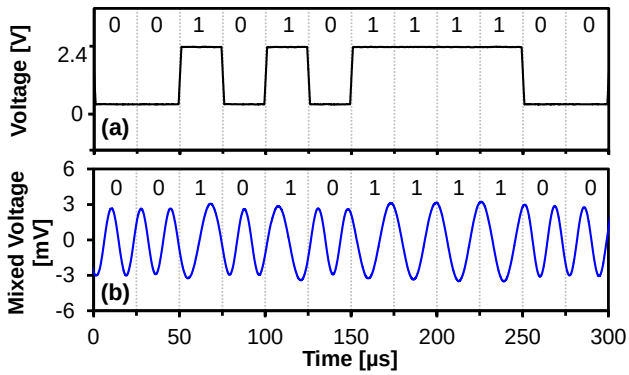

Fig. 10: Applying the 40 kbps modulation bit stream of (a) to the tuning electrodes on one disk array-composite generates the measured FSK modulated waveform of (b), shown mixed down to ~20 kHz to facilitate visualization.

CONTACT: Thura Lin Naing, tel: +1-510-384-4285; thura@eecs.berkeley.edu.